EPJ manuscript No.
(will be inserted by the editor)

Shear-induced Undulation of Smectic-A: Molecular Dynamics Simulations vs. Analytical Theory

Thomas Soddemann[1ab], Günter K. Auernhammer[12c], Hongxia Guo[1], Burkhard Dünweg[1], Kurt Kremer[1]

[1] Max-Planck-Institut für Polymerforschung, D 55021 Mainz, Germany

[2] Theoretische Physik III, Universität Bayreuth, D 95440 Bayreuth, Germany

the date of receipt and acceptance should be inserted later

Abstract. Experiments on a variety of systems have shown that layered liquids are unstable under shear even if the liquid layers are planes of constant velocity. We investigate the stability of smectic-A like liquids under shear using Molecular Dynamics simulations and a macroscopic hydrodynamic theory (including the layer normal *and* the director as independent variables). Both methods show an instability of the layers, which sets in above a critical shear rate. We find a remarkable qualitative and reasonable quantitative agreement between both methods for the spatial homogeneous state and the onset of the instability.

PACS. 61.30.Dk Continuum models and theories of liquid crystal structure – 61.25.Hq Macromolecular and polymer solutions; polymer melts; swelling – 05.70.Ln Nonequilibrium and irreversible thermodynamics – 83.10.Rs Computer simulation of molecular and particle dynamics – 83.50.Ax Steady shear flows, viscometric flow

1 Introduction

Rheological properties of many complex fluids are of widespread interest, *e.g.*, in industrial processing of compound materials or biological applications of lipid membranes.

Subjected to an applied shear flow, layered liquids show an interesting coupling of the layer orientation and the flow field. Experiments on systems which differ significantly in their microscopic details show nevertheless striking similarities in their macroscopic behavior under shear. The systems under investigation include lyotropic lamellar phases (both low molecular weight (LMW) [1–5] and polymeric [6]), LMW liquid crystals (LCs) [7–9],

[a] present address: Rechenzentrum der Max-Planck-Gesellschaft, Boltzmannstraße 2, 85748 Garching, Germany

[b] Thomas.Soddemann@rzg.mpg.de

[c] guenter.auernhammer@mpip-mainz.mpg.de

block copolymers [10–15] and liquid crystalline side-chain polymers [16,17]. In addition to these microscopic differences, the way of applying the shear varies between the systems under consideration. Whereas the highly viscous diblock copolymer melts are usually subjected to a large amplitude oscillatory shear (*e.g.*, in a plate-plate geometry), the low viscosity materials are typically subjected to a steady strain rate (*e.g.*, in a Couette cell). Due to these different experimental methods a direct and quantitative comparison between all the systems mentioned is a non-trivial and open question.

All systems however have in common that starting with an aligned sample where the layers are parallel to the planes of constant velocity ("parallel" orientation), the layering is stable up to a certain critical shear rate [1,2, 6–9,13]. At higher shear rates, depending on the system either multi-lamellar vesicles [1,3,6] ("onions", typically in solvent-rich lyotropic systems) or layers perpendicular to the vorticity direction [13,14,18] (typically in concentrated lyotropic systems and diblock copolymer melts) develop.

The experimental similarities between systems of different molecular constituents indicate that a theoretical description of these reorientations can be constructed—at least to some extent—from a common generic basis. A description including specific differences must refer closer to the microscopic details. The well established standard hydrodynamic description of smectic-A LCs [19–22] is a good macroscopic starting point for such a theoretical approach.

As first shown by Delaye et al. [23] and Clark and Meyer [24] thermotropic smectic-A LCs are very sensitive against dilations of the layers. Above a very small, but finite, value of the dilation the LC develops undulations of the layers to reduce strain locally. Within the framework of standard smectic-A hydrodynamics Oswald and Ben-Abraham considered a situation where a dilative strain is superimposed with a steady shear [25]. When a shear flow is applied (with a parallel orientation of the layers), the onset for undulations is unchanged only if the wave vector of the undulations points in the vorticity direction. Whenever this wave vector has a component in the flow direction, the onset of the undulation instability is augmented by a portion proportional to the applied shear rate. No destabilizing mechanism for well aligned parallel layers is present in standard smectic-A hydrodynamics.

Recently, Auernhammer, Brand and Pleiner proposed an extension of this description [26,27]. Considering both the director of the underlying nematic order and the layer normal of the smectic layers, they showed the possibility of a shear-induced undulation instability due to shear flow even in well aligned parallel layers. Within the framework of irreversible hydrodynamics (which allows the inclusion of both dissipative and reversible effects) they derived the macroscopic dynamic equations of the system and performed a linear stability analysis of these equations. As always, this linear stability analysis is limited to the onset of the first instability. We will review their approach in Sect. 2. In a different approach Bruinsma and Rabin [28] considered the effect of shear flow on the layer fluctu-

ations. They concluded that a destabilization of the layers is likely to occur due to suppressed thermal fluctuations as a result of shear flow. Later a similar approach was used by Zilman and Granek [29], focusing their attention on short wavelength fluctuations. These fluctuations are suppressed in their model for energetic reasons and lead to an undulation instability of the layers. For block copolymers Williams and MacKintosh [30] found by minimizing a free energy of the layers (including shear stress dependent terms) a tendency of these layers to reduce their thickness under shear, leading to an undulation instability similar to dilated smectic-A LCs. Near the isotropic–lamellar transition Fredrickson [31] found the possibility of a parallel to perpendicular transition using a field-theoretic approach and fluctuating hydrodynamic equations. We are not aware of any macroscopic hydrodynamic approach within the framework of the smectic-A like phase besides [26,27].

To our knowledge there has been very little work on simulations of lamellar lyotropic or copolymeric systems under shear flow conditions. Recently, Kumaran et al. used the Lattice Boltzmann simulation method in order to investigate the effect of shear on a smectic liquid crystal [32]. Lamellar layers are introduced into their system as a concentration field. This simulation was however restricted to two dimensions, and hence only able to study shear alignment, but not the undulation instability. Reorientation under applied shear has also been investigated in earlier MD simulations on a similar system [33,34]. In these simulations the layers partially broke apart and reorganized after the reorientation process. No hint for complex defects (like screw dislocations) were found in these simulations. Apparently, much larger systems must be used to study such defects.

In this paper we present a comparison between analytic results obtained by the approach of Auernhammer et al. [26,27] and Molecular Dynamics (MD) simulations of a model system of idealized amphiphiles. We restrict ourselves in the present paper to the analysis of defect-free systems. The results of the simulations show a remarkable qualitative as well as quantitative agreement with the theoretical prediction, but they also pose new questions.

The paper is organized as follows: In Sect. 2 we review the analytic method and give the analytic results. Thereafter (Sect. 3.1) we discuss the simulation technique and present the simulation results in Sect. 3.2. We compare the results of these two approaches and discuss similarities and differences in Sect. 4, followed by some concluding remarks (Sect. 5).

2 Analytical Theory

We assume an idealized shear geometry which is motivated by the simulated system (see Sect. 3.1). As shown in Fig. 1, the layers of the fluid lie in the xy plane and so do the planes of constant velocity. The sample has a thickness d, the uppermost layer moves with a constant velocity $v_0/2$ to the right and the lowermost layer moves with $-v_0/2$ to the left. Thus the system is subjected to a mean shear rate $\dot{\gamma} = v_0/d$. As in the simulated system, we fix only the

mean velocity at the boundaries to the values given above, but no further restriction is imposed on the velocity field.

In a first approach, all systems mentioned in the introduction can be described using the standard formulation of smectic-A hydrodynamics [21]. In this description the layers are assumed to be a two dimensional fluid. Consequently, the layers do not couple directly to the applied shear flow and the observed reorientation cannot be explained using standard smectic-A hydrodynamics. Recently, Auernhammer, Brand and Pleiner [26,27] introduced a new degree of freedom in smectic-A hydrodynamics which allows to describe the destabilization of a parallel aligned sample under an applied shear flow. In the following we will review briefly their model.

2.1 Physical Mechanism

In a smectic liquid crystal one can easily define two directions: the normal to the layers $\hat{p}$ and an average over the molecular axes, the director, $\hat{n}$. In the standard formulation of smectic-A hydrodynamics these two directions are parallel by construction. It has been shown that in the vicinity of phase transitions (either nematic to smectic-A or smectic-A to smectic-C^*) director fluctuations around the layer normal are of physical interest [35–37]. Furthermore, $\hat{n}$ and $\hat{p}$ differ significantly in their interaction with an applied shear flow.

As mentioned above, parallel layers cannot couple directly to an applied shear flow. And so does the layer normal: it stays unchanged as long as the flow direction lies within the layers. In contrast, it is well known from nematic hydrodynamics that the director feels a torque in a shear flow. This torque leads—in the simplest case—to a flow aligning behavior of the director. The key assumption in the model of [26,27] is that a torque of this type is still present in a smectic-A liquid crystal and acts only on the director and not on the layer normal. Both are coupled such that $\hat{n}$ and $\hat{p}$ are parallel in equilibrium.

Subjected to a shear flow the layer normal will stay unchanged, but the director will tilt in the direction of the flow until the torques due to the flow and to the coupling to the layer normal balance one another. For any given shear rate a finite, but usually small, angle θ between $\hat{n}$ and $\hat{p}$ will result. This finite angle has important consequences on the layers: Since the preferred thickness of the layers is proportional to the projection of the director on the layer normal, a finite angle θ between $\hat{n}$ and $\hat{p}$ is equivalent to an effective *dilation* (see Fig. 2) of the layers (the actual layer thickness is larger than the preferred layer thickness)[1]. Roughly speaking, shear has a similar effect on the layers as an external dilation of the system along the layer normal. As in the case of standard smectic-A hydrodynamics [24,23], this effective dilation will lead to a undulation instability of the layers above a certain threshold. Thus the layers can easily fill more space in z direction. Within the framework of standard smectic-

[1] One could argue that the director tilt also leads to a modification of the lateral pressure and the lateral compressibility. For the present system however this effect manifests itself in the same way as the effective dilation (and is included in the appropriate elastic constant).

A hydrodynamics it has been shown (see Ref. [25]) that sheared and dilated systems undulate with a wave vector along the vorticity direction of the flow, *i.e.*, the y direction, see Fig. 1. Since the extended smectic-A hydrodynamics of Refs. [26,27] is equivalent to the standard description in the limit of a vanishing tilt angle θ, we assume the wave vector of the undulations also to lie along the vorticity direction. Later we will show that this assumption is in agreement with the simulation results. The wavelength of this undulation instability is given by the lateral size of the simulation box, since the system has no other large-scale length in vorticity direction.

2.2 Set of Macroscopic Equations

The framework of irreversible thermodynamics [20,22,38, 39] allows to determine the macroscopic hydrodynamic equations of the above model smectic-A [26,27]. A linear stability analysis of these equations directly gives the stability region of the parallel orientation. One should point out that such a linear analysis does not allow any prediction of the pattern formed above the onset of the instability.

Since we consider only small deformations of the parallel orientation, it is convenient to introduce a new variable u (the layer displacement along the z axis) in addition to $\hat{n}$ and $\hat{p}$ (u is connected to $\hat{p}$ via $\hat{p} = [\nabla(z-u)]/[|\nabla(z-u)|]$). Starting from the energy density and the dissipation function of the system, the currents and quasi-currents in the balance equations of all macroscopic variables are derived. To illustrate the idea of the model we will discuss the energy density in some detail. For more details we refer the reader to Refs. [26,27]. Neither the director $\hat{n}$ nor the layer normal does distinguish between head and tail, thus they are required to appear only in even powers in the energy density. Furthermore the energy density of the system is invariant under rigid rotations and homogeneous translations of the whole system.

In the spirit of the model the energy density consists of three parts, a nematic (E_n), a smectic-A (E_s), and a coupling between them (E_c):

$$E = E_n + E_s + E_c. \tag{1}$$

For the nematic and smectic part we adopt the conventional notation, *i.e.*, the Frank free energy density (consisting of splay, twist and bend contribution) and curvature of the layers and layer compression (see, *e.g.*, Ref. [21])

$$E_n = \frac{1}{2}K_1(\nabla\cdot\hat{n})^2 + \frac{1}{2}K_2[\hat{n}\cdot(\nabla\times\hat{n})]^2 + \frac{1}{2}K_3[\hat{n}\times(\nabla\times\hat{n})]^2 \tag{2}$$

$$E_s = \frac{1}{2}K\left(\nabla_\perp^2 u\right)^2, + \frac{1}{2}B_0\left(\nabla_z u\right)^2, \tag{3}$$

with the elastic constants K_1, K_2, K_3, K, and B_0 (connected with nematic splay, twist and bend deformations and smectic layer curvature and layer compression, respectively) and the transverse nabla symbol $\nabla_\perp$ (which includes only the coordinates perpendicular to the preferred direction $\hat{p}$).

As mentioned above, rigid rotations of the system cannot contribute to the energy density due to rotational invariance, but relative rotations of $\hat{n}$ versus $\hat{p}$ may contribute to the energy. Consequently, we assume the cou-

pling term to be quadratic in the angle between $\hat{n}$ and $\hat{p}$. To ensure a positive coupling constant we choose the following version of this term:

$$E_c = \frac{1}{2} B_1 (\hat{n} \times \hat{p})^2. \tag{4}$$

This form has the advantage that is vanishes not only if $\hat{n}$ is parallel to $\hat{p}$ but also for an anti-parallel alignment of both directions. We note that this term, in contrast to the other terms entering the free energy density, is non-hydrodynamic, since it does not vanish in the limit of small wave number excitations (*i.e.*, $q \to 0$). It thus leads dynamically to a relaxation and not to diffusive behavior in the long wavelength limit.

Bend deformations are rather higher order gradient corrections to layer dilations and can be neglected. In the hydrodynamics of smectics twist deformations are forbidden, because in this case no space filling layered structure is possible. In this paper we assume that the angle between $\hat{n}$ and $\hat{p}$ is small and, consequently, also the twist term has to be small and will be neglected. Splay of the director field and layer curvature are very similar deformations, consequently we can combine both into one single term with a new elastic constant (which we call K). Using all these approximations the final form of the free energy density is given by

$$E_{approx} = \frac{1}{2} K \left(\nabla_\perp^2 u\right)^2 + \frac{1}{2} B_0 \left(\nabla_z u\right)^2 + \frac{1}{2} B_1 (\hat{n} \times \hat{p})^2. \tag{5}$$

The other relations used in the derivation of the macroscopic hydrodynamic equations are constructed in the same way, combining nematic and smectic parts. With the standard procedure the balance equations for all hydrodynamic variables can be determined [22,26,27,38]. In the following we assume an incompressible fluid, *i.e.*, a constant mass density ρ. The balance equations for the unknown quantities (the layer displacement u, the director field $\hat{n}$ and the velocity field $\boldsymbol{v}$) are finally given by:

$$\frac{\partial}{\partial t} u + v_j \nabla_j u = v_z + \lambda_p \nabla_j \Psi_j, \tag{6}$$

$$\frac{\partial}{\partial t} n_i + v_j \nabla_j n_i = \lambda_{ijk} \nabla_j v_k - \frac{1}{\gamma_1} \delta_{ik}^\perp h_k, \tag{7}$$

$$\begin{aligned} \rho \left(\frac{\partial}{\partial t} + v_j \nabla_j \right) v_i \\ = & - \nabla_j \left\{ \Psi_j (\nabla_i u - \delta_{iz}) - \lambda_{kji} h_k - \nu_{ijkl} \nabla_l v_k \right\} \\ & - \nabla_i P. \end{aligned} \tag{8}$$

This set of equations is closed by the continuity equation for an incompressible fluid,

$$\nabla_i v_i = 0. \tag{9}$$

For a more compact notation we used in these equations the flow alignment tensor

$$\lambda_{ijk} = 1/2 \left[(\lambda - 1) \delta_{ij}^\perp n_k + (\lambda + 1) \delta_{ik}^\perp n_j \right]$$

along with the flow alignment parameter λ, the transverse Kronecker symbol $\delta_{ij}^\perp = \delta_{ij} - n_i n_j$, the conjugate variables h_i and Ψ_i (related to $\hat{n}$ and ∇u via $h_i = (\delta E)/(\delta n_i)$ and $\Psi_i = (\delta E)/(\delta \nabla_i u)$), the rotational viscosity γ_1^{-1}, the per-

meation constant λ_p, and the viscosity tensor

$$\begin{aligned}\nu_{ijkl} = \quad & \nu_2(\delta_{jl}\delta_{ik} + \delta_{il}\delta_{jk}) \\ & + 2(\nu_1 + \nu_2 - 2\nu_3)n_i n_j n_k n_l \\ & + (\nu_3 - \nu_2)(n_j n_l \delta_{ik} + n_j n_k \delta_{il} \\ & \qquad + n_i n_k \delta_{jl} + n_i n_l \delta_{jk}) \\ & + (\nu_4 - \nu_2)\delta_{ij}\delta_{kl} \\ & + (\nu_5 - \nu_4 + \nu_2)(\delta_{ij} n_k n_l + \delta_{kl} n_i n_j).\end{aligned}$$

The components of vector quantities are indexed, *e.g.*, v_j refers to the components of the velocity field $\boldsymbol{v}$. We make use of the Einstein summation convention.

In the director equation [Eq. (7)] the right hand side expresses the nematic flow alignment and director diffusion. The right hand side of Eq. (8) is the divergence of the stress tensor, which consists of the coupling to the layer displacement (the smectic equivalent to the Erickson stress) and the director (the back-flow term), the viscous terms (containing, as for all uniaxial materials, the five viscosities) and the pressure gradient.

To guarantee the normalization of $\hat{n}$ it is convenient to express $\hat{n}$ in angular variables:

$$n_x = \sin\theta \sin\phi, \tag{10}$$

$$n_y = \sin\theta \sin\phi, \tag{11}$$

$$n_z = \cos\theta. \tag{12}$$

If we denote the right hand side of Eq. (7) with Y_i, the balance equations for θ and ϕ are given by

$$\begin{aligned}\frac{\partial}{\partial t}\theta + v_j\nabla_j\theta = {} & Y_x \cos\theta\cos\phi + Y_y \cos\theta \sin\phi \\ & - Y_z \sin\theta,\end{aligned} \tag{13}$$

$$\frac{\partial}{\partial t}\phi + v_j\nabla_j\phi = -Y_x\frac{\sin\phi}{\sin\theta} + Y_y\frac{\cos\phi}{\sin\theta}. \tag{14}$$

2.3 Director Tilt, Dilation, and Undulations

Before discussing stability of the governing equations, let us focus first on some technical points. Since undulating lamellae lie no longer in the xy plane, their layer normal is no longer parallel to the z axis. To measure the correct layer dilation we must expand $(\partial u)/(\partial z)$ along the current layer normal. The lowest non-trivial expansion leads to the well known replacement [23,24,26]

$$\nabla_z u \to \nabla_z u - \frac{1}{2}\,(\nabla_\perp u)^2 \tag{15}$$

in the energy density of the system. As discussed above, due to the shear induced director tilt the preferred layer thickness is smaller than the actual layer thickness. This effective dilation takes the position of applied dilation in earlier works (see, *e.g.*, Refs.[23,24]). Due to these arguments, the final version of the compression term in the energy density reads

$$\frac{1}{2}B_0\left\{\nabla_z u + [1-\cos\theta] - \frac{1}{2}\,(\nabla_\perp u)^2\right\}^2.$$

The boundary conditions for our further analysis are deduced from the boundary conditions in the simulations. Since the simulation algorithm uses periodic boundary conditions and allows particles to move through the upper and lower boundary, there is no need for the undulation amplitude to vanish at boundaries. We assume this amplitude to be constant throughout the sample. As we will show later, this is in good agreement to the simulation results. Only the average of the x component of the velocity field is controlled in the simulations. So we fix only the average v_x at the upper and lower boundary. Differently to

the undulation instability in an experimental system with rigid boundaries, in the simulated system there is no intrinsic hydrodynamic length scale. The only macroscopic length scale is given by the lateral size of the simulation box ($L_x = L_y = L$).

In the analysis of the above Eqs. (6, 8, 13 and 14) we first look for a spatially homogeneous state and then perform a linear stability analysis of this state. We assume that the boundaries have no direct orienting effect on the director. The preferred homeotropic orientation of the director is only due to the parallel alignment of the layers and the coupling between $\hat{n}$ and $\hat{p}$. This implies that the director field is constant throughout the layer, if $\nabla_z v_x$ is constant. Under these assumptions the linear velocity profile

$$\boldsymbol{v}_0 = \dot{\gamma} z \hat{e}_x \tag{16}$$

satisfies linear momentum conservation Eq. (8) and $\nabla_z v_x$ *is* constant. Inserting this velocity profile in Eq. (13) and supposing an unchanged layered structure leads to the following stationary and spatially homogeneous modifications of the director field:

$$\begin{aligned}\left(\frac{\lambda+1}{2} - \lambda \sin^2(\theta_0)\right)\dot{\gamma} \\ = \quad \frac{B_1}{\gamma_1}\sin(\theta_0)\cos(\theta_0) \\ + \frac{B_0}{\gamma_1}\sin(\theta_0)[1-\cos(\theta_0)].\end{aligned} \tag{17}$$

For small shear rates the director tilt θ_0 is proportional to the applied shear rate:

$$\theta_0 = \dot{\gamma}\frac{\gamma_1}{B_1}\,\frac{\lambda+1}{2} + O(\dot{\gamma}^3). \tag{18}$$

Equation (17) gives a one to one correspondence between shear rate and tilt angle. Thus we can use θ_0 to eliminate the shear rate in the governing equations and take the tilt angle θ_0 as control parameter (instead of the shear rate $\dot{\gamma}$). Whenever necessary we can use Eq. (17) to determine the shear rate for any given tilt angle.

Let us now consider the evolution of the average director field as a function of the applied shear rate. We assume that all variables depend only on the time and the z coordinate and that the shear is such that the layered structure is unaffected by the shear. Averaging the linearized form of Eq. (13) over z, we get

$$\frac{\partial}{\partial t}\langle\theta(t)\rangle = \frac{\lambda+1}{2}\langle\dot{\gamma}(t)\rangle - \frac{B_1}{\gamma_1}\langle\theta(t)\rangle. \tag{19}$$

In Eq. (19) the brackets $\langle\rangle$ indicate the average over z: $\langle\theta(t)\rangle = (1/d)\int_{-d/2}^{d/2}\theta(z,t)dz$ and $\langle\dot{\gamma}(t)\rangle = (1/d)\int_{-d/2}^{d/2}\nabla_z v_x(z,t)dz$. In the discussion of our results we will drop these brackets for simplicity. Note that in the simulations of the following section $\langle\dot{\gamma}(t)\rangle$ is an input parameter and thus is known exactly. After a step like start of the average shear

$$\langle\dot{\gamma}(t)\rangle = \begin{cases} 0, & t \le 0 \\ \dot{\gamma} = \text{const.}, & t > 0 \end{cases} \tag{20}$$

the average director tilt approaches its stationary value with a characteristic time $\tau = \gamma_1/B_1$:

$$\langle\theta(t)\rangle = \dot{\gamma}\frac{\gamma_1(\lambda+1)}{2B_1}\left[1 - \exp\left(-t\frac{B_1}{\gamma_1}\right)\right]. \tag{21}$$

As shown in Fig. 2 this director tilt has important consequences: The non-vanishing projection of $\hat{n}$ on the flow direction directly leads to a z-component of the director $n_z = \cos(\theta)$ less than unity. Following the discussion in Sect. 2.1, this tilt of $\hat{n}$ is equivalent to an effective *dilation* of the layers.

Similar to dilated smectic-A [23,24], this effective dilation will lead to an undulation instability of the layers. We determine the onset of this instability performing a linear stability analysis of the governing equations, *i.e.*, we add to the spatially homogeneous state (see above) small perturbations. For example we replace the spatial homogeneous director tilt θ_0 by

$$\theta_0 \to \theta_0 + \theta_1, \tag{22}$$

with $\theta_1 \ll \theta_0$. Inserting this ansatz in the hydrodynamic equations we can deduce a linear set of equations for the small perturbations (for more details see [27]). For any set of materials parameters it turns out that one can distinguish two regimes of angles θ_0 (and, correspondingly, of shear rates). For small angles the growth rate of the small perturbations is negative for all wave vectors. This means that any perturbation must die out within a certain time, *i.e.*, we expect the system to be stable in the limit of small shear rates. Above a certain threshold value of the tilt angle the layers accommodate the effective dilation by rotating locally, *i.e.*, undulations develop (see Fig. 3). Technically speaking, in this second regime of tilt angles the growth rate of fluctuations within in a certain range of wave vectors becomes positive. In the linear analysis we determine for each wave vector the tilt angle at which the growth rate equals zero and thus we get a curve which separates the the stable from the unstable region (the curve of marginal stability or neutral curve). Minimizing this curve with respect to the wave vector leads to the onset values of the instability (the critical values).

As discussed in Sect. 2.1, for our further calculations we make use of some results about sheared and dilated smectic-A liquid crystals [25]: The critical shear rates is lowest, if the wave vector of the undulations points along the vorticity direction of the flow ($\boldsymbol{q} = q\hat{e}_y$). Note that our system has some important differences in comparison to Ref. [25], namely, the inclusion of the director dynamics and the boundary conditions. In the analytic part of this paper we test for an undulation instability with a wave vector in the vorticity direction. In contrast, the undulations in the simulation form without any assumption about their wave vector and hence justify our choice. Accordingly, our ansatz for the small perturbations in the case of the layer displacement is given by:

$$u_1 = A\cos(qy), \tag{23}$$

with an infinitesimally small amplitude A. A similar ansatz is taken for the other unknown quantities. The absence of an x and z dependence in this ansatz allows to reduce the number of unknown quantities. From the continuity equation it follows directly that $v_{y,1}$ must vanish. Similarly, the perturbations of the director tilt θ_1 and the pressure p_1 can be shown to equal to zero. Consequently, the full set of unknown quantities consists only of the director's azimuthal angle ϕ_1, the layer displacement u_1, the velocity component along the shear flow $v_{x,1}$ and along the unperturbed layer normal $v_{z,1}$.

One might look for a closed expression for the critical tilt angle and expand the solvability condition in powers of θ_0. But it turns out that the simplest physically reasonable approximation includes terms up to $O(\theta^4)$ and,

consequently, any closed expression is rather complicated and of little practical use. Additionally this approximation still differs significantly from the solution of the full system. For these reasons we determine the critical tilt angle numerically and omit the approximative solution.

The reduction in the number of unknown quantities causes also a significant reduction in the number of material parameters necessary for a detailed comparison between analytic theory and MD simulation. To describe the onset of the instability, the set of material parameters consists of the energetic constants B_0, B_1 and K, the flow alignment parameter λ and the viscosity constants γ_1, ν_2 and ν_3. For the comparison with the simulations we can use dimensionless quantities by rescaling the energy density with B_1, the length with the lateral system size L and the viscosities with γ_1.

In Figs. 4 to 6 we present the critical tilt angle above which the undulations set in as a function of various material parameters. For a better comparison with the simulations we used typical values for the system of Sect. 3. If not stated otherwise the parameters were (in dimensionless units) $B_0/B_1 = 6$, $\frac{K}{B_1}\left(\frac{2\pi}{L}\right)^2 = 0.08$, $\lambda = 0.8$,[2] $\nu_i/\gamma_1 = 0.05$ and $\lambda_p/\gamma_1 = 10^{-3}$. We did not present the corresponding plots for ν_i and λ_p, because the critical tilt angle does not depend on this parameters over a wide range of the parameter values.

[2] Note that the a stationary solution also occurs for $|\lambda| < 1$. The tumbling state known from nematics in the range $|\lambda| < 1$ does not occur in our system due to the smectic layering.

To complete the theoretical part let us briefly come back to dilated smectic-A without shear. Following the analysis of [24] and [23] the neutral curve in this case is given by

$$\epsilon = q^2 \frac{K}{B_0}. \tag{24}$$

where ϵ is the relative dilation. Since q is known in the simulated system ($q = 2\pi/L$) we can directly conclude that the critical dilation is

$$\epsilon_c = \left(\frac{2\pi}{L}\right)^2 \frac{K}{B_0}. \tag{25}$$

3 Molecular Dynamics Simulations

3.1 Simulation Model and Methods

For the simulation of our model layered liquids we use a model for amphiphilic systems recently introduced by some of the authors [33]. Its important features are reviewed in the following.

The fluid consists of tetramer chains, where each chain is composed of spherical particles of the same size. We introduce two particle types A and B, such that a tetramer has the structure A-A-B-B, and such that A and B effectively repel each other while like particles attract each other. If this repulsion is strong enough, the system spontaneously forms a lamellar phase. In Ref. [33] the thermodynamic and structural properties of this model were discussed in detail for the case of A-B dimers, while Ref. [34] has studied the non-equilibrium properties of the dimer model under shear. In the present study we have chosen tetramers instead, in order to reduce the diffusion of the

particles perpendicular to the layers. This model can be viewed as a coarse-grained mesoscopic model of diblock copolymers or small surfactants. All particles exhibit a hard core which provides an effective excluded volume. A convenient choice for this is a Lennard–Jones (LJ) potential that is truncated at the minimum, and shifted:

$$U_{LJ} = \begin{cases} 4\,\varepsilon \left[\left(\frac{\sigma}{r}\right)^{12} - \left(\frac{\sigma}{r}\right)^{6} + \frac{1}{4} \right] & r \le 2^{1/6}\sigma \\ 0 & r \ge 2^{1/6}\sigma. \end{cases} \quad (26)$$

The parameters ε and σ give the scales for energy and length. Without loss of generality they can be chosen to be unity in this system.

From polymer simulations it is known that it is computationally efficient to link the particles via anharmonic FENE ("finitely extendible nonlinear elastic") springs with spring constant k and maximum extension R_0:

$$U_{FENE} = \begin{cases} -\frac{1}{2} k R_0^2 \ln \left[1 - \left(\frac{r}{R_0}\right)^2 \right] & r < R_0 \\ \infty & r \ge R_0. \end{cases} \quad (27)$$

The parameters for the FENE potential are chosen to be $k = 5$ and $R_0 = 2.0$.

The effective repulsion between unlike species (*i.e.*, their tendency to unmix if they were not connected) is implemented by introducing an additional attraction between like species [33]. Thus, for A-A and B-B pairs, the original LJ potential, see Eq. (26), is modified to

$$U_{LJcos} = \begin{cases} 4 \left[\left(\frac{1}{r}\right)^{12} - \left(\frac{1}{r}\right)^{6} + \frac{1}{4} \right] - \varphi & r \le 2^{1/6} \\ \frac{1}{2}\varphi \left[\cos(\alpha r^2 + \beta) - 1 \right] & 2^{1/6} \le r \le 1.5 \\ 0 & r \ge 1.5, \end{cases} \quad (28)$$

where φ, the depth of the attractive tail, drives the formation of the lamellar phase, and α and β are chosen to make the potential continuous and differentiable everywhere [33].

For our typical density $\rho = 0.85$ (in terms of monomers), the first-order transition from the disordered to the lamellar phase occurs at $\varphi = 0.78 \pm 0.04$ [40], while the nematic phase is not accessible [41].

The MD simulation is run in the NVT ensemble in a box of size $L_x \times L_y \times L_z$ with periodic boundary conditions. Shear is applied by using the algorithm of F. Müller-Plathe [42]: Two layers at $z = 0$ and $z = L_z/2$ are driven into the $+x$ and $-x$ direction, respectively, see Fig. 7, while the space in between is left untouched (except for the thermostat). The driving is facilitated by suitable exchanges of particle velocities in x direction [42], which works well for large systems, or by a uniform force, which is more suitable for small systems [?]. The amount of driving is continuously adjusted in order to keep the sample-averaged shear rate strictly constant. As a thermostat we use a method analogous to Dissipative Particle Dynamics (DPD) [43]. As discussed in detail in Ref. [?], this is very suitable for shear simulations, since DPD is strictly local, momentum conserving, and Galilei invariant, *i.e.*, fully consistent with hydrodynamics, and thus profile-unbiased. In order to avoid a strong influence on the dynamics a rather small DPD friction parameter was chosen.

Further simulation parameters are: i) temperature $k_B T = 1.0$, ii) strength of the attractive well $\varphi = 1.1$ (deep in the lamellar phase), iii) number of tetramers

$N = 36864$, iv) MD time step $\Delta t = 0.01$. The system was started in a perfectly aligned state. Then the shear rate was increased step by step, where we took the final steady state configuration of the previous run as starting state for the next. By this procedure, we covered the interval $\dot{\gamma} \in [0; 0.025]$.

In order to minimize finite size effects, the box size was carefully adjusted to the layered structure. As checked previously, this procedure guarantees that the thermodynamic properties do not depend on the system size [33, 34]. In the analytic part of the paper we have shown that the wavelength of the undulations is given by the lateral box size. Consequently, one expects that the critical tilt angle depends on the size of the simulated system (see definition of the dimensionless parameters at the end of Sect. 2). In this respect, a variation of the box size would have been desirable but is beyond the scope of the present study.

Note that a step-wise increase in $\dot{\gamma}$ actually means an increase in the average velocity of the driving layers. A new linear profile is established only after some transient time governed by the viscous momentum transport into the sample. After this transient, data in the steady state were taken.

3.2 Simulation Results

Figure 8 shows the shear rate as a function of the director tilt angle. This peculiar form of plotting the simulation data has been used here in order to be able to compare the data directly to the predictions of the theory, especially equation (17), which can only be written as $\dot{\gamma}(\theta_0)$. We observe that, rather than being zero or constant, θ_0 increases with increasing strain rate. A non–zero tilt angle of the director in flow direction means that flow aligning behavior of the director is present; we will discuss this further in the next section.

Up to a strain rate of $\dot{\gamma} = 0.01$, flow alignment is the only response of the director to shear flow. We increased the strain rate further in steps of $\Delta\dot{\gamma} = 0.002$ and we observed undulations in our simulation beyond $\dot{\gamma} = 0.01$. Figure 9 shows a simulation snapshot of the system at a strain rate of $\dot{\gamma} = 0.015$ which clearly exhibits an undulating system with waves in vorticity direction (left to right). The amplitude of the undulation waves, which does not vary along the z axis, has been determined as a function of the shear rate. In order to do this, n_y, the vorticity component of the director, was measured as a function of the y-coordinate. For small amplitudes, the amplitude of the undulations of n_y is proportional to the undulation amplitude of the layers themselves. We are only interested in the general behavior in regard of the magnitude of the amplitude; for this reason the amplitude of the undulations in n_y is a good measure. Figure 10 shows the amplitude of n_y undulations as a function of the shear rate. The non-zero values below a shear rate of $\dot{\gamma} \approx 0.011$ are due to thermal noise, above $\dot{\gamma} \approx 0.011$ the amplitude increases until the layers reorient at $\dot{\gamma} > 0.025$.

For a better understanding of the system we will compare the simulation results reported above to a dilation "experiment" where the system gets dilated in one direc-

tion, along the layer normal in our case, while the lateral dimension are kept constant. At low dilation no effect of the stretching is observable, beyond a certain percentage of elongation ϵ of the simulation box undulations of the layers set in. The undulation amplitude can be measured in the same way as in the case of shear and the results are shown in Fig. 11. The onset for those undulations takes place at a $\epsilon = 1.9\%$ stretching. The amplitude of the undulations increases until roughly 3% dilation. Beyond 3% the layers of the non–isochoric dilated system become unstable and break apart. Note that in this latter case, the undulations occur in both x and y direction.

4 Discussion

The simulation results of the preceeding section are quite obviously very similar to the picture developed using the analytic theory. The most outstanding similarities are the presence of the director tilt and the onset of an undulation instability above a threshold value for the shear rate. In this section we will present a more detailed comparison between the results of Secs. 2 and 3. With the performed simulations we are able to determine almost all the dimensionless parameters of the system without making use of the onset of the undulation instability. This in turn enables a check of the set of parameters by comparing the observed (simulated) undulation threshold to the threshold predicted by the analytic theory (using the material parameters).

We start our discussion with the stationary and dynamic behavior of the director tilt below the onset of undulations. In the analytical part we showed that the time dependence of the average director tilt after a step like start of the shear will approach its stationary value within a characteristic time given by $\tau = \gamma_1/B_1$ [see Eq. (21)]. Figure 12 gives a comparison of the time evolution of the average director tilt after a step like start of the shear for different shear rates. Note that in the simulations the average shear rate is given as input parameter and the director measured is the average director. The time to establish the average shear is short compared with the characteristic time associated with the director tilt. Since Eq. (21) is only valid for small θ we must restrict our analysis of the numerical data to small shear rates. Both shear rates used lead to the same values for B_1/γ_1 and λ, namely,

$$\frac{B_1}{\gamma_1} = 0.045 \pm 0.004, \tag{29}$$

$$\lambda = 0.88 \pm 0.1. \tag{30}$$

In principle most of the parameters could be derived from a fit of Eq. (17) to the data plotted in Fig. 8, where we show the stationary response of the director tilt as a function of shear rate. But it turns out that such a fit is rather imprecise. Instead, we use the previously derived flow alignment parameter to reduce the uncertainty in the fit. The value for B_1/γ_1 in this fit is consistent with the results to Fig. 12. Following this procedure we can derive the last undetermined parameter of Eq. (17)

$$\frac{B_0}{\gamma_1} = 0.22 \pm 0.14 \tag{31}$$

With the results for B_0/γ_1 and B_1/γ_1 at hand we can provide now an estimate for the ratio B_0/B_1.

$$\frac{B_0}{B_1} = 5.3 \pm 3.4 \tag{32}$$

Let us turn for a moment to the simulations of the dilated system where no shear is present. Those show an onset of the undulation instability at a dilation of about 2%. Assuming a square root dependence of the amplitude beyond onset we get (see dashed line in Fig. 11)

$$\epsilon_c = 1.6\% \pm 0.2\% \tag{33}$$

Inserting this value along with the estimate from above for B_0/γ_1 in Eq. (25) we obtain

$$\frac{K}{B_1}\left(\frac{2\pi}{L}\right)^2 = 0.085 \pm 0.055. \tag{34}$$

Besides the renormalized viscosities ν_i/γ_1 all relevant parameters are now determined. The analytical theory predicts only a slight influence of the viscosities on the onset of undulations as long as $\nu_i/\gamma_1 \gtrsim 0.05$. If we assume this relation to hold, the predicted threshold value for the undulation instability is

$$\theta_c = 0.35\ ^{+0.45}_{-0.20}. \tag{35}$$

For a good estimate of the critical shear rate we assume a square root dependence of the undulations amplitude and, thus, find a simulated critical shear rate of

$$\dot{\gamma}_{c,\mathrm{sim}} = 0.0103 \pm 0.0007. \tag{36}$$

Transforming this simulated threshold value with Eq. (17) and the above parameters, we find the simulated critical tilt angle to be

$$\theta_{c,\mathrm{sim}} = 0.18 \pm 0.02 \tag{37}$$

Thus, we can conclude that, within the error bars, the analytic theory is in qualitative as well as reasonable quantitative agreement with the simulation results in the range of validity of the linear theory.

5 Conclusion

In this paper we have shown that the director (as defined in a nematic liquid crystal) has its own independent dynamics in the smectic-A phase. To do so we have used two independent methods, namely, a linear stability analysis of the macroscopic, hydrodynamic equations [26,27] and a molecular dynamics simulation of a model bilayer smectic-A [33]. The simulation of this model system for layered liquids shows, above a critical shear rate, an undulation instability, which arises spontaneously. The analytic theory tests for the stability of the spatially homogenous state against undulations and also finds a critical shear rate. Despite the differences in the approaches, both methods (molecular dynamics simulations and analytic theory) are in good qualitative and reasonable quantitative agreement in the range of validity of both methods. At low shear rates we observe a director tilt in the simulations which corresponds to analytical predictions. Increasing the shear rate above a critical value leads (in the simulations and in the analytic theory) to an undulation instability of the layers. Using a number of further simulations on the same system, we can determine an (almost complete) set of material parameters for the simulated system independent of the threshold value of the tilt angle. Inserting these parameters in the analytical calculations we can show that both methods are in agreement within the error bars. For many purposes, we conclude that the accessible size of the simulated systems is now in the range covered by continuum approaches (as, *e.g.*, hydrodynamic theory) and the

comparison between both kinds of approaches may have stimulating effects for both fields.

The authors thank the European Commission for support through TMR grant number ERB FMGE CT950051 (TRACS Program at Edinburgh Parallel Computer Center). For one of us (GKA) it is a pleasure to thank the Deutsche Forschungsgemeinschaft for partial support of this work through SFB 481 "Komplexe Makromolekül- und Hybridsysteme in inneren und äußeren Feldern". The authors acknowledge gratefully fruitful and stimulating discussions with Helmut R. Brand, Harald Pleiner, and Jürgen Vollmer.

References

1. O. Diat, D. Roux, and F. Nallet, J. Phys. II France **3**, 1427 (1993).
2. S. Müller, C. Börschig, W. Gronski, C. Schmidt, and D. Roux, Langmuir **15**, 7558 (1999).
3. J. I. Escalante and H. Hoffmann, Rheol. Acta **39**, 209 (2000).
4. J. Zipel, F. Nettesheim, P. Linder, T. D. Le, U. Olsson, and W. Richtering, Europhys. Lett. **53**, 335 (2001).
5. F. Nettesheim, J. Zipfel, U. Olsson, F. Renth, P. Lindner, and W. Richtering, Langmuir **19**, 3603 (2003).
6. J. Zipfel, P. Lindner, M. Tsianou, P. Alexandridis, and W. Richtering, Langmuir **15**, 2599 (1999).
7. R. G. Horn and M. Kléman, Ann. Phys. (France) **3**, 229 (1978).
8. C. R. Safinya, E. B. Sirota, and R. J. Plano, Phys. Rev. Lett. **66**, 1986 (1991).
9. P. Panizza, P. Archambault, and D. Roux, J. Phys. II France **5**, 303 (1995).
10. V. K. Gupta, R. Krishnamoorti, Z.-R. Chen, J. A. Kornfield, S. D. Smith, M. Satkowski, and J. T. Grothaus, Macromolecules **29**, 875 (1996).
11. U. Wiesner, Macromol. Chem. Phys. **198**, 3319 (1997).
12. J. H. Laurer, B. Scott Pinheiro, D. L. Polis, and K. I. Winey, Macromolecules **32**, 4999 (1999).
13. J. L. Zryd and W. R. Burghardt, Macromolecules **31**, 3656 (1998).
14. H. Leist, D. Maring, T. Thurn-Albrecht, and U. Wiesner, J. Chem. Phys. **110**, 8225 (1999).
15. D. L. Polis, S. Smith, N. J. Terrill, A. J. Ryan, D. C. Morse, and K. I. Winey, Macromolecules **32**, 4668 (1999).
16. L. Noirez and A. Lapp, Phys. Rev. Lett. **78**, 70 (1997).
17. L. Noirez, Phys. Rev. Lett. **84**, 2164 (2000).
18. J. Zipfel, J. Berghausen, G. Schmidt, P. Lindner, P. Alexandridis, M. Tsianou, and W. Richtering, Phys. Chem. Chem. Phys. **1**, 3905 (1999).
19. P. G. de Gennes, Solid State Commun. **10**, 753 (1972).
20. P. C. Martin, O. Parodi, and P. S. Pershan, Phys. Rev. A **6**, 2401 (1972).
21. P. G. de Gennes and J. Prost, *The Physics of Liquid Crystals* (Clarendon Press, Oxford, 1993).
22. H. Pleiner and H. R. Brand, in *Pattern Formation in Liquid Crystals*, edited by A. Buka and L. Kramer (Springer, New York, 1996), Chap. 2, Hydrodynamics and Electrohydrodynamics of Liquid Crystals.
23. M. Delaye, R. Ribotta, and G. Durand, Phys. Lett. **44A**, 139 (1973).
24. N. A. Clark and R. B. Meyer, Appl. Phys. Lett. **22**, 493 (1973).
25. P. Oswald and S. I. Ben-Abraham, J. Phys. France **43**, 1193 (1982).

26. G. K. Auernhammer, H. R. Brand, and H. Pleiner, Rheol. Acta **39**, 215 (2000).
27. G. K. Auernhammer, H. R. Brand, and H. Pleiner, Phys. Rev. E **66**, 061707 (2002).
28. R. Bruinsma and Y. Rabin, Phys. Rev. A **45**, 994 (1992).
29. A. G. Zilman and R. Granek, Eur. Phys. J. B **11**, 593 (1999).
30. D. R. M. Williams and F. C. MacKintosh, Macromolecules **27**, 7677 (1994).
31. G. H. Frederickson, J. Rheol. **38**, 1045 (1994).
32. V. Kumaran, S. Jariwala, and S. Hussain, Chem. Eng. Sci. **56**, 5663 (2001).
33. T. Soddemann, B. Dünweg, and K. Kremer, Eur. Phys. J. E **6**, 409 (2001).
34. H. Guo, K. Kremer, and T. Soddemann, Phys. Rev. E **66**, 061503 (2002).
35. P. G. de Gennes, Mol. Cryst. Liq. Cryst. **21**, 49 (1973).
36. J. D. Litster, J. Als-Nielson, R. J. Birgeneau, S. S. Dana, D. Davidov, F. Garcia-Golding, M. Kaplan, C. R. Safinya, and R. Schaetzing, J. Phys. Coll. C3 **40**, C3 (1979).
37. S. Garoff and R. B. Meyer, Phys. Rev. Lett. **38**, 848 (1977).
38. S. R. de Groot and P. Mazur, *Non-equilibrium Thermodynamics* (North-Holland, Amsterdam, 1962).
39. D. Forster, *Hydrodynamic Fluctuations, Broken Symmetries, and Correlation Functions* (W. A. Benjamin, Reading, Massachusetts, 1975).
40. H. Guo and K. Kremer, J. Chem. Phys. (in press).
41. D. Morse and S. Milner, Phys. Rev. E **47**, 1119 (1993).
42. F. Müller-Plathe, Phys. Rev. E **59**, 4894 (1999).
43. P. Español and P. Warren, Europhys. Lett. **30**, 191 (1995).

FIGURES

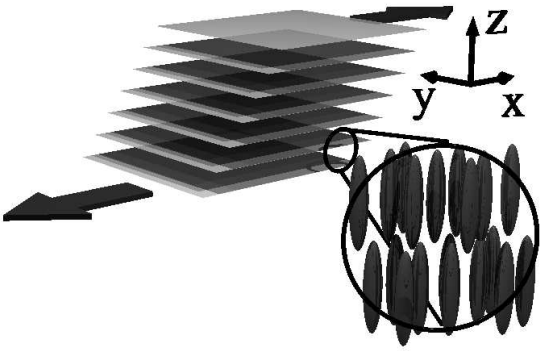

Fig. 1. In the analytical part of this paper we consider a laterally infinite layer with the uppermost and lowermost layer moving in opposite directions, but with equal velocity. The depicted molecules illustrate the principal structure and are not meant to give any microscopic detail.

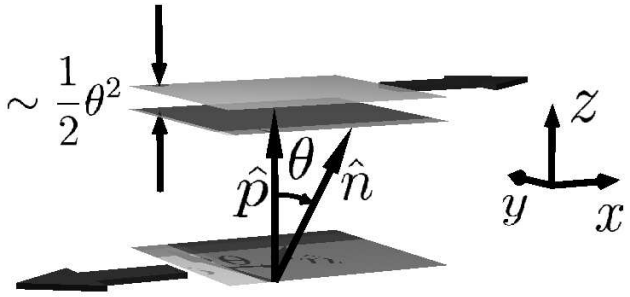

Fig. 2. A finite angle between $\hat{n}$ and $\hat{p}$ leads to a tendency of the layers to reduce their thickness. Supposing a constant number of layers in the sample, this tendency is equivalent to an effective dilation along the layer normal. For small angles between $\hat{n}$ and $\hat{p}$ the relative effective dilation is given by $\frac{1}{2}\theta^2$ (picture taken from Ref. [27]).

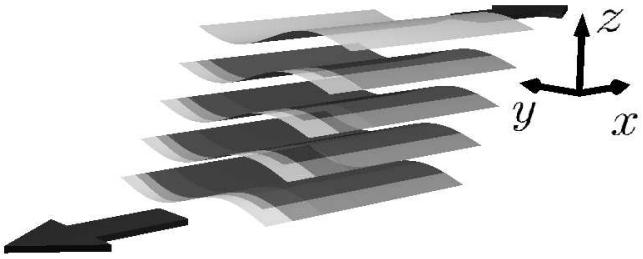

Fig. 3. Above a certain threshold, the effective dilation due to the director tilt will lead to undulations of the layers. Note the difference in directions: The director is tilted in the flow direction, whereas the wave vector points along the y axis. This configuration cancels the direct coupling between the flow and the undulations.

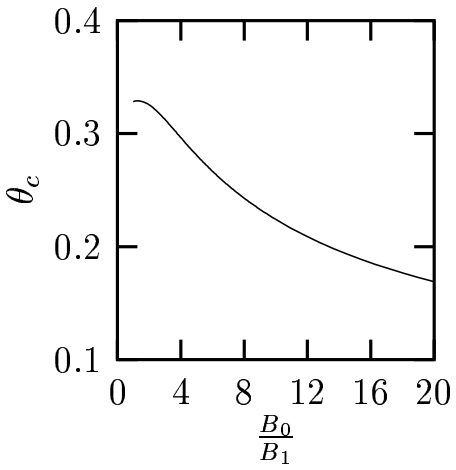

Fig. 4. Critical tilt angle versus the dimensionless compression modulus of the layers (see text for further comments).

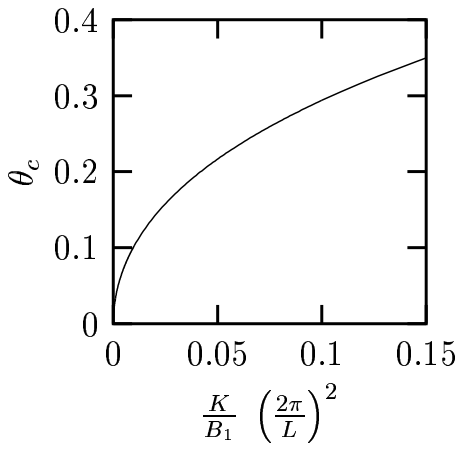

Fig. 6. Critical tilt angle versus the dimensionless bending modulus of the layers.

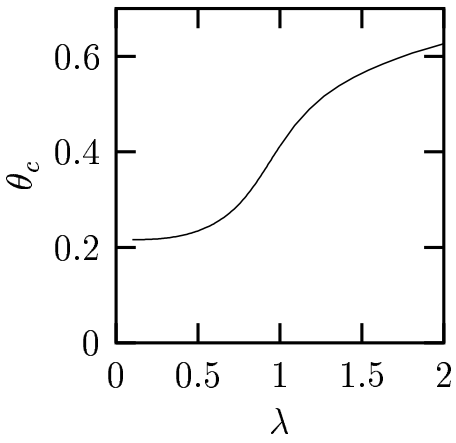

Fig. 5. In the relevant parameter range the critical tilting angle increases with λ.

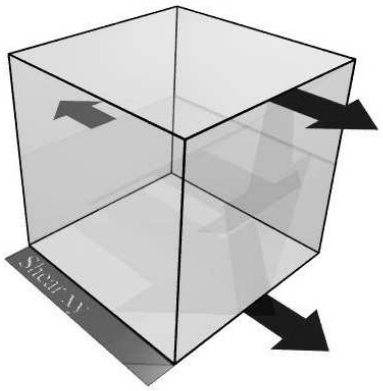

Fig. 7. Orientation of the shear flow in the simulation. The maximum flow directions are sketched by the arrows. The shear at the bottom is equal to the periodic image above the top of the box. The middle slab is moving in opposite direction. Note that both, the upper and the lower half of the simulated system correspond on their own to the system considered in Sect. 2.

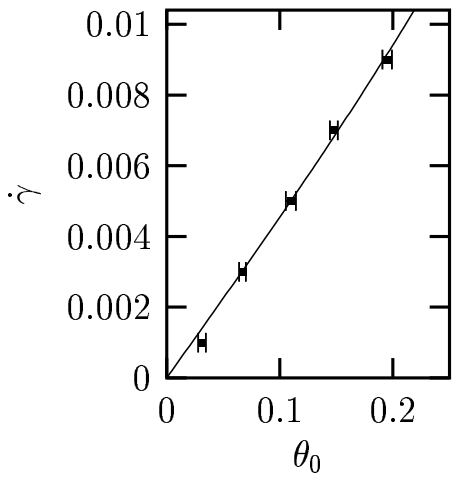

Fig. 8. Strain rate as a function of the tilt angle. This peculiar form of presenting the data has been chosen in order to facilitate a direct comparison with the theory, especially Eq. (17). The solid line is a fit of this equation to the data (see Sect. 4 for more details).

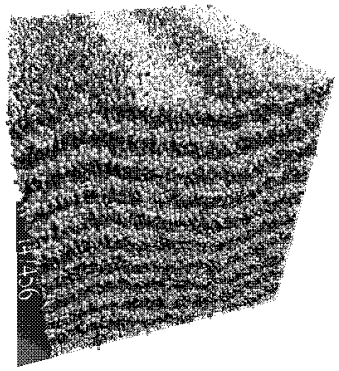

Fig. 9. Undulations in the simulated model system. At a strain rate of $\dot{\gamma} = 0.015$ clearly undulations have developed. As considered in the theory, undulations in the vorticity direction are present. Note that the undulation amplitude does not change along the z axis.

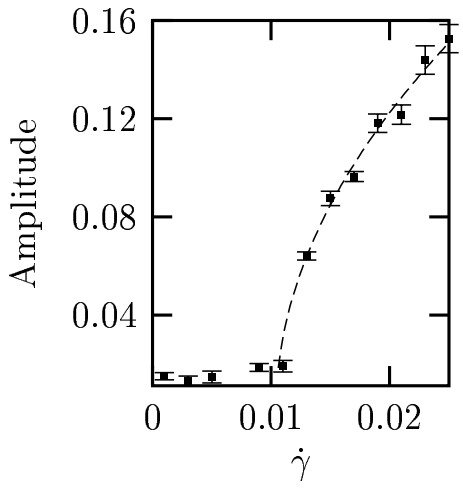

Fig. 10. Undulation amplitude due to shear. The amplitude of the undulations A is given as a function of the strain rate $\dot{\gamma}$. At a shear rate of $\dot{\gamma} \approx 0.01$ undulations set in. The amplitude of these undulations grows continuously with increasing shear rate. The dashed line shows a fit to data points starting at $\dot{\gamma} > 0.01$ assuming a square root dependence of the amplitude above the undulation onset.

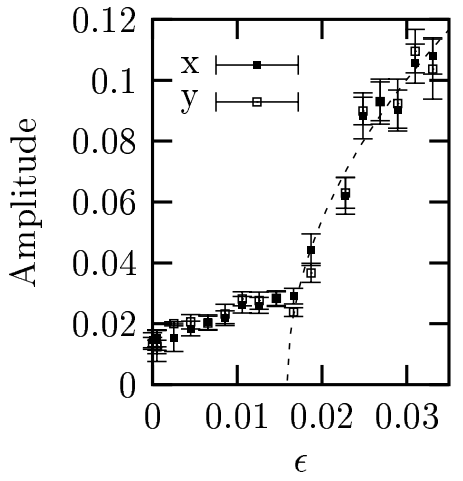

Fig. 11. Undulation amplitude as a function of the dilation ϵ. For values of the dilation of $\epsilon \approx 0.019$ the system starts to respond with undulations and the amplitude increases continuously until the layers break apart for $\epsilon > 3\%$. The dashed line (- - -) shows a fit to the data points assuming a square root dependence of the amplitude above onset.

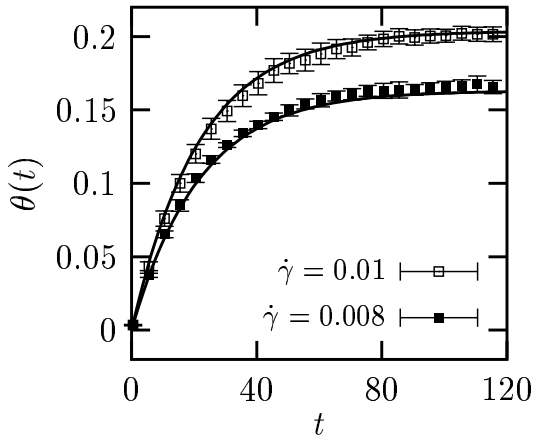

Fig. 12. Time evolution of the director tilt after a step like start of the shear for two different final shear rates (0.008 and 0.010 in Lennard-Jones units). The lines show the fit to the data using Eq. (21).